Chinese Chemical Letters 34 (2023) 107680

Contents lists available at ScienceDirect

Chinese Chemical Letters

journal homepage: www.elsevier.com/locate/cclet

Biointerface engineering of self-protective bionic nanomissiles for targeted synergistic chemotherapy

Xueyan Zhen[a,b], Linhao Li[a,b], Lanlan Jia[a,b], Aihong Zhu[a,b], Yixuan Yang[a,b], Sicen Wang[a,b], Xiaoyu Xie[a,b,*]

[a] School of Pharmacy, Health Science Center, Xi'an Jiaotong University, Xi'an 710061, China
[b] Shaanxi Engineering Research Center of Cardiovascular Drugs Screening & Analysis, Xi'an 710061, China

ARTICLE INFO

Article history:
Received 24 January 2022
Revised 11 July 2022
Accepted 12 July 2022
Available online 14 July 2022

Keywords:
Aptamer
Self-protective
Biointerface
Targeted drug delivery
Synergistic chemotherapy

ABSTRACT

Erythrocyte membrane (EM)-camouflaged chemotherapeutic delivery nanovehicles hold promise for solid tumor therapy because of their excellent biostability and biocompatibility. However, it is accompanied with insufficient targeting effect and deficient pharmacokinetic behavior due to the lack of a regulated biointerface to navigate and overcome biological transportation obstacles in solid tumor therapy. Herein, an anti-epidermal growth factor receptor (EGFR) aptamer (EApt) modified and EM-cloaked chemotherapeutic nanomissile delivery system was constructed. The anchored-EApt acting as a specific EGFR suppressor promotes to inhibit the overexpression of EGFR and initiate the cell apoptosis. Importantly, the resulting PLGA-DOX@EM-EApt orchestrated the bioactivity of each component and provided synergistic cell apoptosis and antitumor effects by precisely suppressing EGFR expression levels and delivering DOX. The *in vitro* and *in vivo* experimental results confirmed that the immune escape and active targeting behaviors of PLGA-DOX@EM-EApt could significantly promote its drug retention and tumor inhibition abilities. Our findings propose a novel strategy using the biointerface functionalization technique, demonstrating a promising therapeutic platform *via* a biomimetic drug delivery system for precise solid tumor recognition and synergistic therapy.

As the first-line agents for cancer therapy, single chemotherapeutics remains cytotoxic against solid tumors with insufficient doses to diseased regions [1], thereby inducing numerous side effects and hindering their antitumor efficacy further [2]. Recently, biomimetic nanomaterials with superior characteristics have been developed to mimic the physicochemical properties of intrinsic cells and serve as drug nanocarriers to treat a variety of diseases [3]. In particular, erythrocyte membrane (EM), the essential unit of the structure and function of erythrocytes, has aroused wide interest in cancer nanotherapy [4]. Recent advances in EM-camouflaged techniques can be utilized to efficiently promote the biocompatibility and pharmacokinetic behaviors and avoid the immunogenicity of nanomaterials in an organism [5]. However, increasing evidence highlights the obstacles faced by these EM-derived nanocarriers in solid tumor therapy, such as insufficient targeting effects and unacceptable pharmacokinetics. Therefore, it would be highly desirable to extend the specificity and validity of EM-biointerface to overcome the long-standing challenges in treatment strategies.

Currently, regulation of cell membrane biointerface *via* surface engineering techniques has been increasingly used in various biomedical applications [6,7]. Among them, the binding of biological molecules on the cell membrane of biomimetic nanocarriers by external stimuli has been widely utilized to endow them with the dynamic recognition capability of receptors on the targeted cells [8,9]. For example, to accurately promote the functional effects and bioactivity of the biointerface, efficient engineering ligands such as exogenous polysaccharides [10], antibodies [11], enzymes [12], peptides [13], and nucleic acid aptamers [14] have been introduced without compromising the original membrane functions. Therein, aptamers, superior ligands with intrinsic programmability and biocompatibility engineered on the biointerface, have attracted great attention in mediating diverse cellular behaviors, including the control of cell adhesion or apoptosis [15]. Despite the outrageous achievements made in engineering biointerface, the limitations in combining specific aptamer-engineered techniques with further applications in solid tumor therapy still exist. Given the superiority of EM-camouflaged drug nanocarriers, introducing aptamers to EM could regulate the interactions between self-protective drug-

* Corresponding author at: School of Pharmacy, Health Science Center, Xi'an Jiaotong University, Xi'an 710061, China.
E-mail address: xiexiaoyu@xjtu.edu.cn (X. Xie).

https://doi.org/10.1016/j.cclet.2022.07.023
1001-8417/

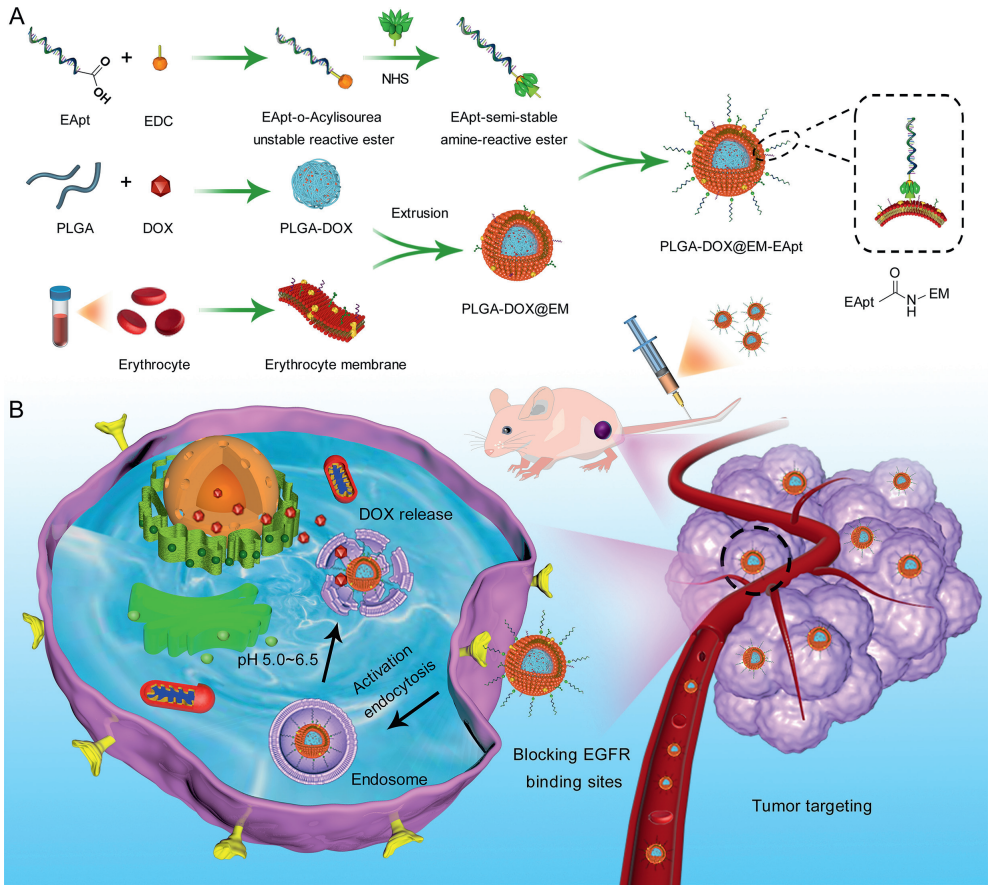

Fig. 1. Schematic illustration of (A) the preparation of biomimetic PLGA-DOX@EM-EApt nanomissiles and (B) the mechanism of EGFR-targeted and synergetic therapy against solid breast tumor by combing EApt-mediated cell apoptosis and chemotherapy.

loaded nanomaterials and the targeting locations, which could be envisioned as a feasible cancer therapy method.

Epidermal growth factor receptor (EGFR), a potential prognostic biomarker for chemotherapeutic delivery in EGFR-positive cancers [16], is involved in activating downstream signal transduction pathways [17] and is overexpressed in a wide variety of tumor cells [18]. Therefore, suppressing the gene expression of EGFR on the cell membrane represents a plausible strategy to inhibit the malignancy of EGFR-positive tumors. The selected anti-EGFR aptamer (EApt), a single-stranded DNA (ssDNA) molecule with high binding specificity and antitumor ability [19], can specifically recognize and block EGFR binding sites on the extracellular domain, followed by initiating the activation of the endocytosis signal pathway mediated by the translocation of EGFR into the lysosomes for degradation [20], thereby decreasing the expression of EGFR on the cell membrane. Therefore, EApt acting as a specific EGFR suppressor anchored on the nanomissiles could lead to the promotion of cell apoptosis. Due to the excellent biocompatibility [21], enhanced cell penetration [22] and weak immune response [23], EApt-conjugated nanocomposite is becoming an emerging alternative to specifically deliver therapeutic agents to EGFR-overexpressing tumor sites.

Herein, we reported an EGFR-targeted chemotherapeutic nanomissile coated with EApt-modified EM (denoted as PLGA-DOX@EM-EApt) (Fig. 1A), whose active targeting ability and cancer therapeutic efficacy were systematically investigated. *In vitro* and *in vivo* experiments confirmed that this newly-designed PLGA-DOX@EM-EApt exhibited specific targeting capability, long circulation half-life and low intrinsic immunogenicity, which together enriched doxorubicin (DOX) delivery in EGFR-overexpressing solid breast tumor cells. Simultaneously, the self-protective PLGA-DOX@EM-EApt nanomissiles executed a two-edged sword function of inducing targeted drug delivery and cell apoptosis mediated by EApt, followed by a specific chemotherapy to promote triple negative breast cancer cell death (Fig. 1B).

To construct self-protective bionic nanomissiles, PLGA-DOX was first fused and enveloped by EM to obtain EM-cloaked PLGA-DOX@EM. Notably, PLGA here is a kind of biodegradable pharmaceutical excipient with the property of hypotoxicity and sustained-release of drugs. The drug-loaded PLGA-DOX avoid the damage of complement system and plasma to the drugs and nanocarriers, which is conducive to transport the drugs and take effect more stable. Then, a stable EApt was introduced to the biointerface of PLGA-DOX@EM (Fig. 2A). As illustrated in Fig. S1A (Supporting information), EApt modified with carboxyl groups was introduced to finally form stable amide bonds between the amino groups on the EM by covalent conjugation. Transmission electron microscopy (TEM) images exhibited the typical and well-maintained core-shell structures of PLGA-DOX@EM and PLGA-DOX@EM-EApt nanomissiles (Fig. 2B). The hydrodynamic size was examined, and the final diameter of PLGA-DOX@EM and PLGA-DOX@EM-EApt at the optimized EM-to-PLGA-DOX mass ratio of 1.0 (Fig. 2E) was around 10 nm thicker than that of bare PLGA-DOX, validating the successful coating of the EM (Fig. 2C). The zeta potential of PLGA-DOX@EM and PLGA-DOX@EM-EApt increased approximately 20 mV (Fig. 2D), which resulted from the EM shield on the negative carboxyl groups of the PLGA-DOX core. Additionally, as shown in Figs. S1B and C (Supporting information), the most appropriate amount of EApt conjugated onto EM was finally determined to be 200 μL. The UV-vis absorption peaks of the EM-EApt solution were consistent with free EApt (290 nm) and EM (260 nm) solutions

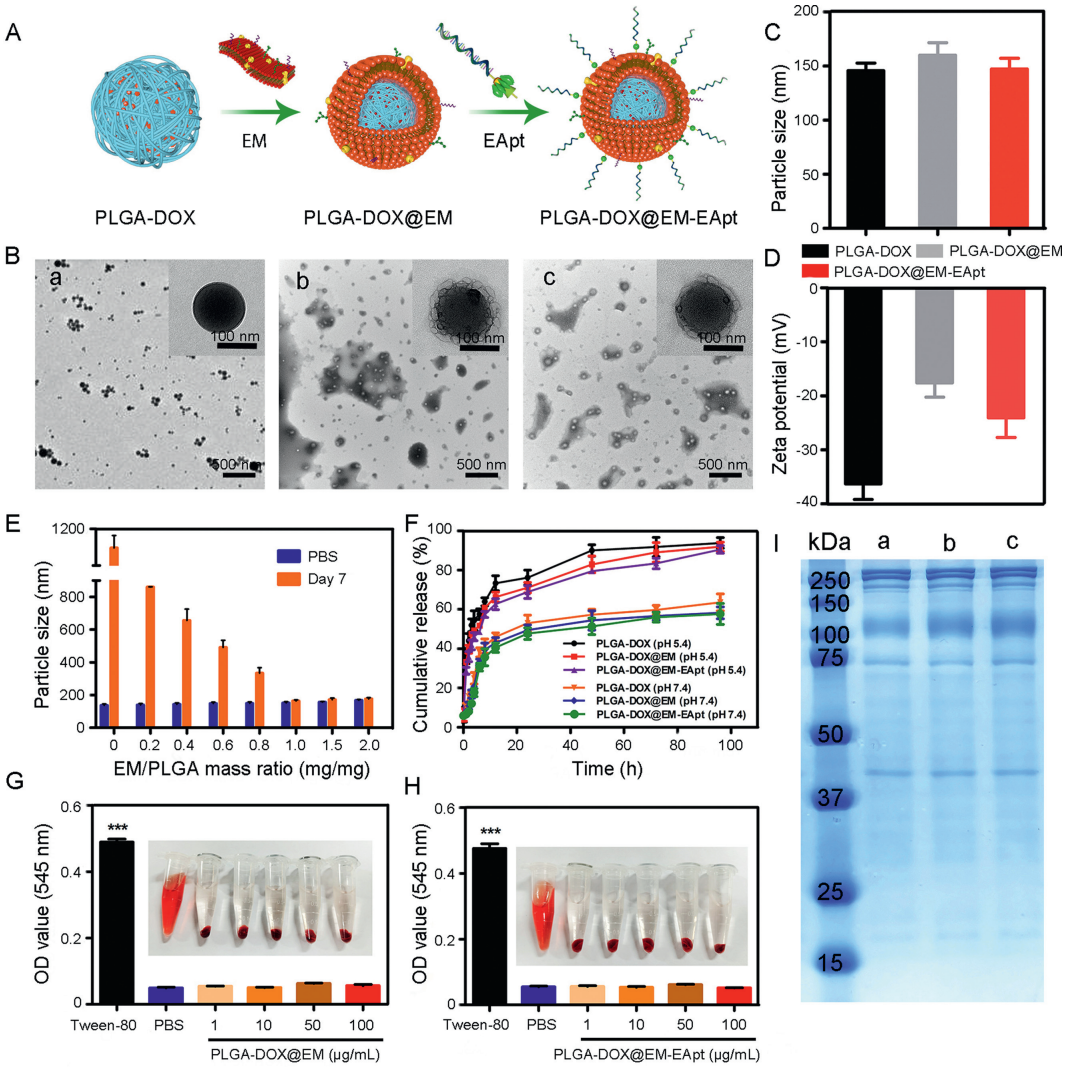

Fig. 2. Fabrication, characterization, and biocompatibility of PLGA-DOX@EM-EApt nanomissiles. (A) Schematic illustration of the preparation of PLGA-DOX@EM-EApt. (B) TEM images of (a) PLGA-DOX, (b) PLGA-DOX@EM and (c) PLGA-DOX@EM-EApt. Scale bars: 500 nm; inset: 100 nm. (C) Average particle diameters and (D) surface ζ-potentials of different nanomissiles. (E) Optimization of EM/PLGA mass ratio through mean particle diameters analysis. (F) Accumulative DOX release proportion from various as-prepared nanomissiles under different pH conditions. Hemolytic analysis of (G) PLGA-DOX@EM and (H) PLGA-DOX@EM-EApt. (I) SDS-PAGE analysis of EM proteins extracted from (a) PLGA-DOX@EM-EApt, (b) PLGA-DOX@EM and (c) EM.

(Fig. S2 in Supporting information), suggesting that EApt was eventually conjugated onto the EM. The successful anchoring between EApt and EM was also evaluated by fluorescence colocalization (Fig. S3 in Supporting information). Besides, the X-ray diffraction (XRD) pattern records for PLGA-DOX and PLGA-DOX@EM-EApt were displayed in Fig. S4 (Supporting information), suggesting that the structure of PLGA-DOX was essentially maintained during the EM cloaking process. As shown in Fig. S5 (Supporting information), the Fourier transform infrared (FT-IR) spectrum of EApt-semi-stable amine-reactive ester displayed peaks at 1749 cm^{-1} and 1248 cm^{-1}, which were consistent with the ester groups. And the spectrum of EM-EApt included peaks at 1689 cm^{-1} assigned to amido bond C=O, 1531 cm^{-1} and 1290 cm^{-1} assigned to N-H. These results verified the successful formation of EApt-semi-stable amine-reactive ester. Moreover, the increased intensity at 3300 cm^{-1} band further demonstrated that EApt was conjugated onto the EM. In addition, as shown in Table S1 (Supporting information), 2 mg DOX was finally chosen to prepare PLGA-DOX@EM-EApt with preferable encapsulation efficiency and loading content.

PLGA-DOX@EM and PLGA-DOX@EM-EApt groups exhibited the similar protein reservation as EM (Fig. 2I), demonstrating the successful translocation of original EM proteins. Then, the uptake efficiency of Raw 264.7 cells was evaluated. The fluorescence exhibited in PLGA-DOX@EM and PLGA-DOX@EM-EApt groups was weaker than that in the PLGA-DOX group (Fig. S10A in Supporting information). Similarly, the quantitative outcome of flow cytometry showed that the fluorescence intensity of PLGA-DOX group was twice higher than those of the other groups (Figs. S10B and C in Supporting information), confirming that the self-recognized proteins expressed on EM could suppress the uptake by macrophage cells.

In vitro DOX release kinetics of PLGA-DOX, PLGA-DOX@EM, and PLGA-DOX@EM-EApt were determined. A higher cumulative DOX release profile was measured in phosphate buffer saline (PBS) at pH 5.4 than that at pH 7.4 in the first 24 h (Fig. 2F), indicating that the weak acidic atmosphere could rapidly increase the dissociation of the formulations and subsequent diffusion of the loaded DOX. Additionally, the stability of different formulations was analyzed through monitoring the changes in particle size, polydispersity index (PDI) in PBS (Fig. S6 in Supporting information), and absorbance values in PBS or fetal bovine serum (FBS) (Fig. S7 in Supporting information). These results together demonstrated that

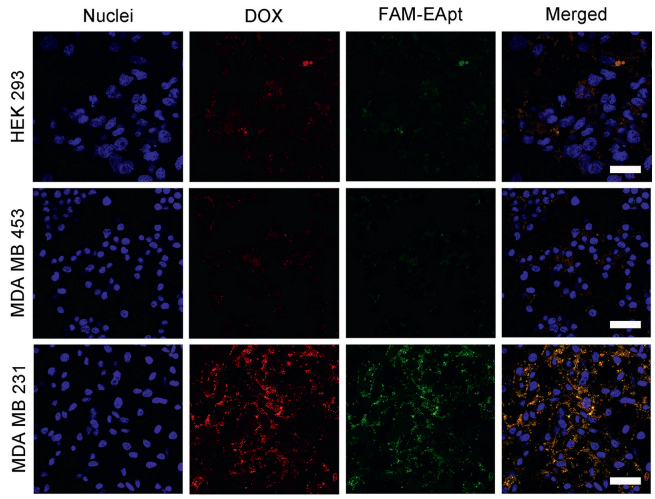

Fig. 3. CLSM images of HEK 293, MDA MB 453 and MDA MB 231 cells treated with PLGA-DOX@EM-FAM-EApt. Blue: nuclei. Red: DOX. Green: EApt modified with FAM. Scale bars: 50 μm.

EM coating prevented nanoparticle agglomeration and enhanced the stability of PLGA-DOX@EM and PLGA-DOX@EM-EApt.

The compatibility of the materials was systematically investigated. The blood supernatants incubated with PLGA-DOX@EM and PLGA-DOX@EM-EApt were transparent, and their absorbance values were similar to that of the negative control group (PBS) (Figs. 2G and H). Besides, the platelet adhesion test was also performed to evaluate the hemocompatibility. As shown in Fig. S8 (Supporting information), the platelet adhesion rates of the blood incubated with PLGA-DOX@EM and PLGA-DOX@EM-EApt were similar to that of control group, which is lower than PLGA-DOX group. These results indicated that PLGA-DOX@EM and PLGA-DOX@EM-EApt with EM-coating exhibited an excellent blood compatibility. We next investigated the cytotoxicity of PLGA and PLGA@EM by standard MTT assay. The cytocompatibility results (Figs. S10D-F in Supporting information) revealed cell viability was above 80%, and no significant cytotoxicity was observed.

The cellular targeting recognition behavior of PLGA-DOX@EM-EApt was evaluated *via* exposure to three types of cells. The EGFR-overexpressing MDA MB 231 cells, EGFR-negative MDA MB 453 cells and EGFR-negative HEK 293 cells were selected for following investigation (Fig. S9 in Supporting information). Then the cell-specific recognition and internalization capabilities were observed. As shown in Fig. 3, MDA MB 231 cells phagocytosed a relatively larger amount of PLGA-DOX@EM-EApt than those ingested by the other cells, indicating the efficiently targeting recognition and cellular internalization efficacy of PLGA-DOX@EM-EApt. Thus, PLGA-DOX@EM-EApt, with powered and guided properties, is capable of precisely locking and hitting the target, which is why we called it 'nanomissile'.

We also revealed the specific recognition mechanism of PLGA-DOX@EM-EApt. The intracellular internalization of PLGA@DiI-EM-EApt was obviously improved (Fig. S11A in Supporting information), whereas the uptake of PLGA@DiI-EM-EApt by cells pre-incubated with free EApt decreased, indicating that reduction was mediated by the competitive blocking and inhibition of EGFR with the addition of free EApt, and the quantitative flow cytometry exhibited a similar phenomenon (Figs. S11B and C in Supporting information).

We next investigated the drug delivery efficacy of PLGA-DOX@EM-EApt. Evident DOX red fluorescence was observed in MDA MB 231 cells treated with PLGA-DOX@EM-EApt (Fig. S15A in Supporting information), whereas the weak fluorescence was recorded in HEK 293 (Fig. S12 in Supporting information) and MDA MB 453 cells (Fig. S13 in Supporting information), indicating the excellent targeting recognition and drug accumulation ability of PLGA-DOX@EM-EApt. Flow cytometric analysis was also conducted to quantify the amount of DOX accumulation (Figs. S15B and S14 in Supporting information). Due to the targeted recognition efficacy of EApt, there was an obvious increase of fluorescence intensity after PLGA-DOX@EM-EApt treatment in MDA MB 321 cells (Fig. S15C in Supporting information) compared to that in MDA MB 453 and HEK 293 cells. Moreover, a large amount of the internalized PLGA-DOX@EM-EApt was observed to co-localize in lysosomes in the perinuclear regions after treatment (Fig. S16 in Supporting information), which finally indicated that the intracellular drug transport behavior was regulated by the acidic lysosome environment.

Then we examined the EGFR expression level in MDA MB 231 cells treated with DOX, PLGA-DOX@EM, PLGA@EM-EApt, and PLGA-DOX@EM-EApt, respectively. The protein level of EGFR was significantly downregulated in the PLGA@EM-EApt and PLGA-DOX@EM-EApt groups (Fig. S17 in Supporting information). Therefore, EApt could specifically bind to EGFR and decrease the expression level of EGFR. Furthermore, the apoptosis of MDA MB 231 cells was effectively induced by PLGA-DOX@EM-EApt (69.89%) (Fig. S18 in Supporting information), which confirmed a more significant cell apoptosis effect than that in EGFR-negative MDA MB 453 cells (16.40%) (Fig. S19 in Supporting information). Collectively, these results verified that EApt was employed to block the EGFR binding sites on cell membrane and activate the endocytosis signal pathway, ultimately leading to enhanced apoptosis. Moreover, as shown in Fig. S20 (Supporting information), the DOX, PLGA-DOX@EM and PLGA@EM-EApt groups exhibited dose-dependent inhibition in both MDA MB 231 and MDA MB 453 cells. The 50% inhibitory concentration (IC_{50}) of PLGA-DOX@EM-EApt in MDA MB 231 cells was 7.343 μg/mL, which was much lower than that in MDA MB 453 cells, validating the sufficient cytotoxicity and effective antitumor efficacy.

To study the circulation of the nanomissiles *in vivo*, the pharmacokinetic assay was conducted. All animal operations were permitted by the Ethics Committee of Biomedicine of Xi'an Jiaotong University Health Science Center (No. 2020-169). Within the pre-determined administration time, the DOX group exhibited a rapid clearance from the circulation system (Fig. S22B in Supporting information), whereas the PLGA-DOX@EM and PLGA-DOX@EM-EApt groups displayed a markedly increased retention of DOX in blood. The pharmacokinetic parameter results suggested the prolonged circulation time and decreased DOX clearance profiles of PLGA-DOX@EM and PLGA-DOX@EM-EApt groups (Fig. S21 and Table S2 in Supporting information), which were attributed to the EM coating-induced decreased immune elimination.

The tumor-specific delivery *in vivo* was performed to verify the targeting distribution. MDA-MB-231 tumor-bearing mice were administrated with DOX, PLGA-DOX, PLGA-DOX@EM and PLGA-DOX@EM-EApt, respectively (Fig. S22A in Supporting information). As shown in Fig. S22C (Supporting information), the PLGA-DOX@EM-EApt group displayed the highest fluorescence intensity at the tumor site (marked with yellow circle in Fig. S22D in Supporting information) at 8 h, providing evidence for targeted binding between PLGA-DOX@EM-EApt and EGFR overexpressed on the MDA MB 231 cells. Additionally, the tumors and major organs were removed for fluorescence imaging (Fig. S22E in Supporting information). The observed fluorescence intensity at the tumor area in the PLGA-DOX@EM-EApt group was much higher than that in the other groups due to the active delivery to tumor area instead of the enhancing permeation and retention (EPR) effect.

In vivo antitumor properties of PLGA-DOX@EM-EApt were investigated. As described in Figs. 4A-C, tumor growth was significantly inhibited after PLGA-DOX@EM-EApt treatment. In Fig. 4D,

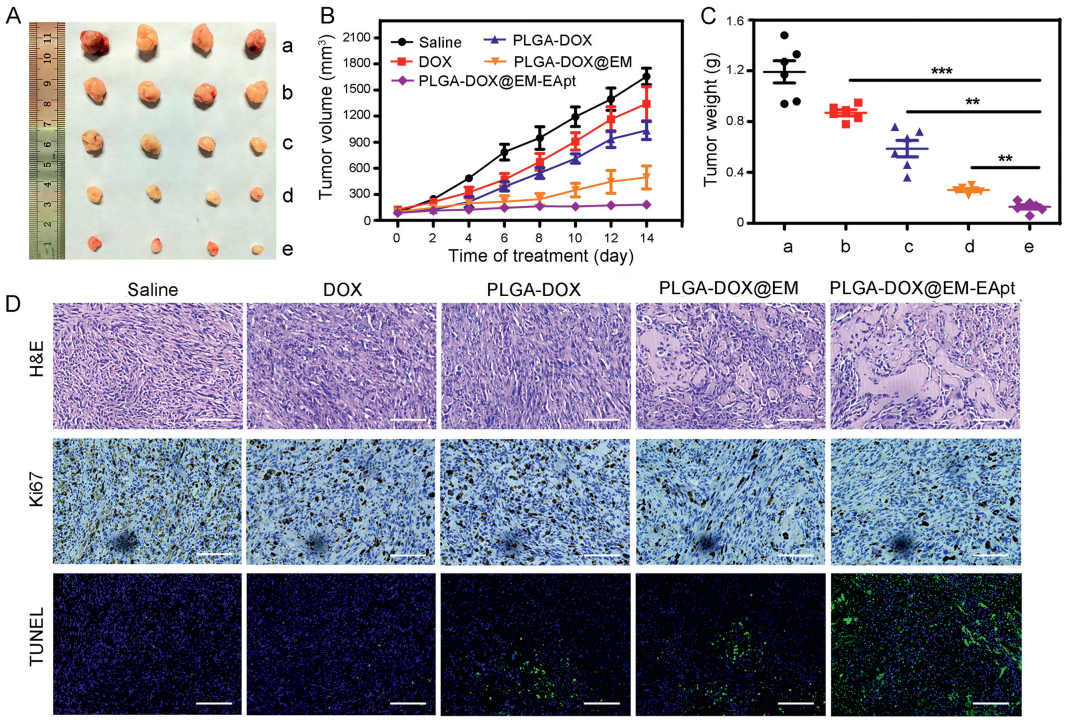

Fig. 4. *In vivo* therapeutic application in synergistic antitumor efficacy. (A) Representative photographs of tumors harvested from MDA MB 231 tumor-bearing mice treated with (a) saline, (b) DOX, (c) PLGA-DOX, (d) PLGA-DOX@EM and (e) PLGA-DOX@EM-EApt for 14 days. Tumor (B) volume and (C) weight in the mice receiving different treatments. Values are means ± SD (**$P < 0.01$, ***$P < 0.001$). (D) Histological observation and measurement of apoptosis in the tumor sections after therapy. Scale bars: 100 μm.

tumor sections were analyzed by hematoxylin and eosin (H&E), Ki-67 (a tumor progression indicator) and terminal-deoxynucleoitidyl transferase mediated nick end labeling (TUNEL) staining. Significant damage, disintegration and apoptosis of tumor cells were observed in the PLGA-DOX@EM-EApt group, suggesting the precise targeting transportation of DOX and subsequent tumor accumulation attributed to EApt-mediated enhanced penetration after PLGA-DOX@EM-EApt treatment.

In vivo biological safety assessment of PLGA-DOX@EM-EApt was examined. The bodyweight of the mice remained stable during the therapy except for those treated with DOX, which was attributed to the myocardial tissue damage induced by free DOX (Fig. S23A in Supporting information). More than 60% of the mice treated with PLGA-DOX@EM and PLGA-DOX@EM-EApt were still alive on day 60 (Fig. S23B). Moreover, the main toxic effect of heart-like cardiomyopathy was found in the DOX-treated mice (Fig. S24 in Supporting information). The blood biochemistry parameters were measured to evaluate the functions of the main organs, and the results indicated the significant damage to the heart and liver (Fig. S23C in Supporting information). Collectively, these results consistently demonstrated highly-effective and less-toxic PLGA-DOX@EM-EApt treatment *in vivo*, illustrating excellent biocompatibility and weakened immune-recognition ability due to the EM-cloaking and EApt-conjugation.

In summary, we designed and fabricated a promising EM-inspired self-protective nanomissile PLGA-DOX@EM-EApt by combining the smart merits of EApt-engineered biointerface and biomimetic chemotherapeutic delivery system, which endowed the nanomissiles with efficacious capability of precise and synergistic solid tumor therapy. Because of employing the biological surface engineering techniques, PLGA-DOX@EM-EApt was intelligently capable of modulating tumor-targeting drug delivery through specific interaction with EGFR proteins, leading to the regulated cancer cell apoptosis and synergistic breast cancer therapy, which thus simultaneously executed a two-edged sword function. Meanwhile, the excellent biocompatibility and effective tumor-targeting ability of PLGA-DOX@EM-EApt were demonstrated at both the cell and animal levels, and the results revealed that engineering the biological EApt molecule on the biointerface of the EM-based self-protective nanocarriers would provide a new ground for further applications in tumor treatment. Overall, this design highlights a potential and multifunctional drug delivery strategy and provides new guidance on manipulating the functionalities of biointerface for synergistic cancer therapy.

Declaration of competing interest

The authors declare that they have no known competing financial interests or personal relationships that could have appeared to influence the work reported in this paper.

Acknowledgments

This work was supported by the National Natural Science Foundation of China (Nos. 82073807 and 81973277) and the World-Class Universities (Disciplines) and the Characteristic Development Guidance Funds for the Central Universities, China (No. PY3A012). We thank Dr Hao at the Instrument Analysis Center of Xi'an Jiaotong University for the assistance with CLSM analysis and Dr Zhao at the Biomedical Experimental Center of Xi'an Jiaotong University for the assistance with IVIS analysis.

Supplementary materials

Supplementary material associated with this article can be found, in the online version, at doi:10.1016/j.cclet.2022.07.023.

References

[1] N.V. Du, H.K. Min, H.Y. Kim, et al., ACS Nano 15 (2021) 8492–8506.
[2] Y.X. Sun, W.H. Zhai, X.J. Liu, et al., Theranostics 9 (2019) 5828–5838.

[3] H.L. Wang, Y.F. Zhu, L.L Zhang, et al., Chin. Chem. Lett. 33 (2022) 2937–2941.
[4] H. Liu, Z.H. Miao, Z.B. Zha, Chin. Chem. Lett. 33 (2022) 1673–1680.
[5] R.F. Ke, X.Y. Zhen, H.S. Wang, et al., J. Colloid Interface Sci. 609 (2022) 307–319.
[6] Y.S. Bu, X.L. Zhang, A.H. Zhu, et al., Anal. Chem. 93 (2021) 7898–7907.
[7] Q. Hu, L.L. Jia, X.L. Zhang, et al., Acta Pharm. Sin. B 12 (2021) 394–405.
[8] Z.L. Chai, D.N. Ran, L.W. Lu, et al., ACS Nano 13 (2019) 5591–5601.
[9] X.L. Liu, X. Zhong, C. Li, Chin. Chem. Lett. 32 (2021) 2347–2358.
[10] C. Lee, R. Verma, S. Byun, et al., Nat. Commun. 12 (2021) 3611.
[11] X. Wei, Z.Y. Feng, J.B. Huang, et al., ACS Appl. Mater. Int. 13 (2021) 32810–32822.
[12] H. Zhang, Y.H. Xia, F. Wang, et al., Adv. Sci. 8 (2021) 2003404.
[13] C. Xu, S. Yang, Z.J. Jiang, J. Zhou, J. Yao, Nano Lett. 20 (2020) 372–383.
[14] S.P. He, F. Gao, J.H. Ma, et al., Angew. Chem. Int. Ed. 60 (2021) 23299–23305.
[15] L. Kashefi-Kheyrabadi, J. Kim, S. Chakravarty, et al., Biosens. Bioelectron. 169 (2020) 112622.
[16] Q. Hu, X.L. Zhang, L.L. Jia, et al., Biomater. Sci. 8 (2020) 5690–5697.
[17] E.L. Morgan, J.A. Scarth, M.R. Patterson, et al., Cell Death Differ. 28 (2021) 1669–1687.
[18] P. Jain, C.D. Shanthamurthy, P.M. Chaudhary, R. Kikkeri, Chem. Sci. 12 (2021) 4021–4027.
[19] T.T. Lv, Z.Y. Li, L. Xu, et al., Acta Biomater. 76 (2018) 257–274.
[20] W.J. Ma, Y.X. Zhang, Y.X. Zhang, et al., Nano Lett. 19 (2019) 4505–4517.
[21] T.X.Z. Liang, Z.G. Yao, J. Ding, et al., ACS Appl. Mater. Int. 10 (2018) 34050–34059.
[22] Y. Chen, Z.H. Li, P. Pan, R.Y. Zeng, X.Z. Zhang, ACS Nano 15 (2021) 11514–11525.
[23] C. Ipilimuma, S. Camorani, C. Vetrei, et al., Cancers 12 (2020) 331.